Unification of the Rheological Physics of Yield Stress Fluids

Krutarth Kamani, Gavin J. Donley, and Simon A. Rogers[*]

Department of Chemical and Biomolecular Engineering, University of Illinois at Urbana-Champaign, Illinois 61801, USA

The physics above and below the yield stress is unified by a simple model for viscoplasticity that accounts for the nonlinear rheology of multiple yield stress fluids. The model has a rate-dependent relaxation time, allows for plastic deformation below the yield stress, and indicates that rapid elastic deformation aids yielding. A range of commonly observed rheological behaviors are predicted, including the smooth overshoot in the loss modulus and the recently discovered contributions from recoverable and unrecoverable strains in amplitude sweeps.

Yield stress fluids change from being viscoelastic solids, where deformations are recoverable, to deforming plastically, where deformation is unrecoverable, as an applied load is increased beyond a threshold. Yielding is most often associated with glasses, gels, and jammed systems. Soft materials with structures as diverse as foams, microgel suspensions, emulsions, pastes, and granular suspensions [1–13], as well as polymer networks, colloidal gels, capillary suspensions, and magnetorheological fluids [14–22], have all been shown to yield.

Despite the fact that yield stress fluids (YSFs) are made from various microstructural elements, their bulk rheology displays many similarities, suggesting that a common continuum description is possible.

A conceptually simple illustration of yielding behavior is elicited by the application of a constant shear rate to a previously at-rest YSF. An elastic behavior is observed at small stresses and strains and is followed by yielding and stable flow after a threshold stress or strain is exceeded [23–25].

When a range of constant stresses are applied, the viscosity of YSFs bifurcates about the yield stress, with the viscosity diverging for stresses below the yielding condition and remaining finite and stable above it. This behavior has been shown to manifest as avalanche behavior during inclined plane tests [26–31].

Under dynamic testing conditions achieved by oscillating the applied strain, the response of YSFs is more complex. Under small-amplitude oscillatory shear (SAOS), the dynamic moduli, which reflect energy storage and dissipation, are nearly independent of frequency. As the strain amplitude is increased, a smooth overshoot is observed in the loss modulus, followed at larger amplitudes by a decrease in both moduli [32–37]. The overshoot in the loss modulus has recently been shown to be due to a transition in how strain is acquired, from predominantly recoverable (elastic) at small amplitudes to predominantly unrecoverable (plastic) at larger amplitudes [38], without a clear indication of a single yield point [39,40]. The range of behaviors exhibited under strain-controlled conditions has made determination of a single well-defined yield point difficult [41].

Experiments that resolve structural-level information, such as diffusing-wave spectroscopy [42], rheo-microscopy 43]], ultrasonic speckle velocimetry [44–47], and rheo-scattering [48,49], have indicated that yielding is a gradual behavior, and that irreversible rearrangements take place below the yield stress [50–56].

Yielding is typically modeled at the continuum level in terms of a critical stress, below which it is assumed that no plastic flow occurs. Prior to yielding, YSFs have been described as being perfectly rigid, elastic, or viscoelastic solids [57]. In the plastic regime, the stress is typically described as a combination of a yield stress term and some flow condition, which typically takes the form of a generalized Newtonian flow [4,58–65]. This has led to discontinuous piecewise descriptions of YSF rheology [57,66,67], referred to as the Oldroyd-Prager formulation [41,66,68,69], in which the preyielded solid behavior is described by different physics to the plastic state. The discontinuity of the piecewise description is often discarded in computational studies of flows in complex geometries, in favor of regularized models that treat the behavior of YSFs as purely viscous [70–73].

In this Letter, we unify the rheological physics above and below the yield stress by constructing a continuum model of YSF rheology that avoids the piecewise nature of the Oldroyd-Prager formulation. We show that its predictions account for experimental results from a range of rheological protocols on a model YSF.

The rheology of soft materials in general, and YSFs in particular, can be decomposed into a sum of recoverable and unrecoverable shear strain and rate components [38,74–77],

$$\gamma(t) = \gamma_{\text{rec}}(t) + \gamma_{\text{unrec}}(t), \tag{1}$$

218002-1

$$\dot{\gamma}(t) = \dot{\gamma}_{\text{rec}}(t) + \dot{\gamma}_{\text{unrec}}(t), \qquad (2)$$

where γ_{rec} and γ_{unrec} are the recoverable and unrecoverable shear strains, and $\dot{\gamma}_{\text{rec}}$ and $\dot{\gamma}_{\text{unrec}}$ are their rates. The recoverable component is related to elastic processes, while the unrecoverable component is related to the plastic behavior [74,75,78,79]. We use the concepts of strain and rate decomposition to build our model.

In the linear viscoelastic regime, when YSFs are in their unyielded solid states, the dynamic moduli $G'(\omega)$ and $G''(\omega)$ are observed to be weakly or negligibly dependent on the frequency [35,37,80], with $G'(\omega) \gg G''(\omega)$. We therefore prescribe that the recoverable component of the model be a viscoelastic solid element with an elastic modulus $G = G'(\omega)$ and a structural viscosity $\eta_s = G''(\omega)/\omega$.

Steady flow experiments at long times probe the unrecoverable, or plastic acquisition of strain. In this Letter, we use a Herschel-Bulkley representation of the steady-shear viscosity [59], which includes a yield stress σ_y, a consistency index k, and an exponent n, such that the plastic viscosity $\eta_p(\dot{\gamma}) = \sigma_y/|\dot{\gamma}| + k|\dot{\gamma}|^{n-1}$. Other variants of the steady shear behavior of YSFs could also be used [61].

We construct the model so that the plastic viscosity η_p is dependent on the total shear rate, which includes the rate at which strain is acquired recoverably, $\dot{\gamma}(t) = \dot{\gamma}_{\text{rec}}(t) + \dot{\gamma}_{\text{unrec}}(t)$. The dependence is prescribed by the steady-shear behavior. The strong shear-rate dependence of the plastic viscosity means that plastic deformation is assisted by the rate at which elastic deformation is acquired and also that plastic flow can occur transiently below the yield stress, as observed experimentally [42–49].

The complete model is

$$\sigma + \lambda(\dot{\gamma})\dot{\sigma} = \left(\frac{\sigma_y}{|\dot{\gamma}|} + k|\dot{\gamma}|^{n-1} \right) \left(\dot{\gamma} + \frac{\eta_s}{G}\ddot{\gamma} \right), \qquad (3)$$

where $\lambda(\dot{\gamma})$ is the rate-dependent relaxation time that is a consequence of combining the recoverable and unrecoverable components,

$$\lambda(\dot{\gamma}) = \frac{\frac{\sigma_y}{|\dot{\gamma}|} + k|\dot{\gamma}|^{n-1} + \eta_s}{G}. \qquad (4)$$

A rate-dependent relaxation time was recently observed in the yielding behavior of amorphous solid colloidal monolayers [81]. For simplicity, we have shown here only the evolution of the shear component of the extra stress tensor. A full tensorial version of the model (see Supplemental Material [82] for details), also includes an expression for the evolution of the first normal stress difference, which predicts the quadratic dependence on the shear stress that was observed recently [85]. The model predicts no second normal stress difference.

This model describes the physical behavior above and below the yield stress in a single equation, in direct contrast

to the Oldroyd-Prager formulation, and hence unifies the physics that governs the yielded and unyielded behavior. While a single steady-state yield stress is assumed, the process of yielding is accounted for by the rate-dependent relaxation time $\lambda(\dot{\gamma})$, and can therefore be thought of as a viscoelastic process. The model parameters are obtained from two steady-state tests, but account for a wide range of transient behaviors, as we will show.

We compare the predictions of the model, which were obtained numerically using MATLAB, to experimental rheological data collected from a simple yield stress fluid: a polymer microgel—Carbopol 980, 1 wt% (see Supplemental Material [82]). We also show results for two other YSFs in the SI: a biopolymer suspension—xanthan gum, 4 wt% (see Supplemental Material [82] for material preparation); and a dense (glassy) colloidal suspension—concentrated Ludox TM-50, 42 vol% (see Supplemental Material [82] for material preparation). These materials are known to display thixotropy and aging [86–89] and yet the simple model, which does not attempt to describe either effect, captures the main features of their yielding behavior. The rheometrical geometries used were chosen to replicate existing works in the literature [38] (see Supplemental Material [82] for details).

All measurements were made with an Anton Paar Modular Compact Rheometer (MCR) 702, operating in single-drive mode. This instrument's electronically commutated synchronous motor allows for experiments to be carried out under stress-controlled and strain-controlled modes, with rapid switching between the two over intervals of a few milliseconds.

Linear-regime frequency sweeps were performed at a strain amplitude of $\gamma_0 = 0.00316$ strain units to obtain the model parameters related to recoverable components of the model, with G and η_s determined from the dynamic moduli at $\omega = 1$ rad/s with $G = G'$ and $\eta_s = G''/\omega$. The steady shear flow curve is fit by the Herschel-Bulkley model. Model parameter values are listed in the Supplemental Material [82].

Oscillatory shear tests were performed at an angular frequency $\omega = 1$ rad/s, over the strain amplitude range $0.006 \leq \gamma_0 \leq 10$ to create an amplitude sweep. Data from additional frequencies are shown in the Supplemental Material [82]. Measurements were made at steady alternance, once all initial transience had decayed. An iterative constrained recovery procedure was employed at 40 distinct evenly spaced instants during an oscillation (see [38,78] for a detailed experimental protocol) to obtain recoverable and unrecoverable components at each amplitude.

A comparison of the experimental data and model predictions for amplitude sweeps are shown in Fig. 1(a) for Carbopol 980. A smooth overshoot in the loss modulus is observed at intermediate amplitudes, followed by the decrease of both moduli at the largest amplitudes. The smooth transitions in the experimentally determined
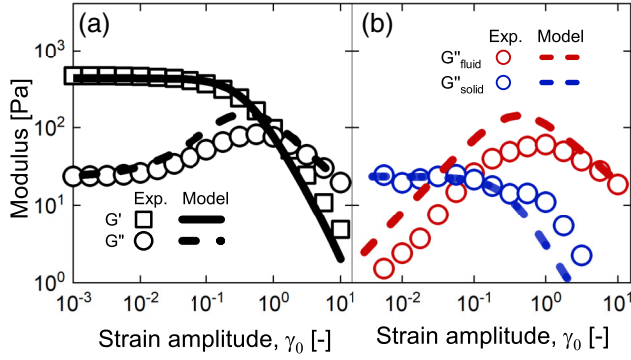
FIG. 1. (a) The dynamic moduli $G'(\gamma_0)$ and $G''(\gamma_0)$ as functions of strain amplitude for Carbopol. (b) Components of the loss modulus $G''_{\text{solid}}(\gamma_0)$ and $G''_{\text{fluid}}(\gamma_0)$ corresponding to dissipation from recoverable and unrecoverable strains. Symbols are experimental data; lines are model predictions. Model parameters are listed in the Supplemental Material [82].
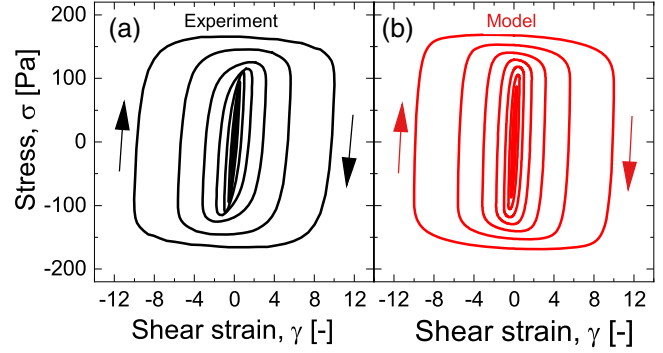

FIG. 2. Comparison of the elastic Lissajous curves from the amplitude sweep at $\omega = 1$ rad/s for Carbopol 980 between the experiments (a) and the model (b). Model parameters are listed in the Supplemental Material [82].

moduli are accurately captured by the model through the rate-dependent relaxation time $\lambda(\dot{\gamma})$. At small strain amplitudes and moderate frequencies, where the applied shear rate remains low, the relaxation time is always longer than the period of oscillation, and the response remains solidlike. As the applied shear rate increases at larger amplitudes, the relaxation time decreases, and more fluidlike behavior is elicited.

The dynamic moduli physically represent the average energy stored and dissipated per cycle [79]. Energy dissipation can be associated with the rate at which recoverable elastic strain is acquired,

$$G''_{\text{solid}}(\omega, \gamma_0) = 2[\dot{\gamma}_{\text{rec}}(t)\sigma(t)]_{\text{avg}}/\omega\gamma_0^2, \qquad (5)$$

as well as the rate at which unrecoverable plastic strain is acquired,

$$G''_{\text{fluid}}(\omega, \gamma_0) = 2[\dot{\gamma}_{\text{unrec}}(t)\sigma(t)]_{\text{avg}}/\omega\gamma_0^2. \qquad (6)$$

While $G''(\omega, \gamma_0)$ includes contributions from both recoverable and unrecoverable modes, the overshoot is due to unrecoverable modes only [38]. We show in Fig. 1(b) that the predictions of the model are very close to the experimentally determined energy dissipation components [38], $G''_{\text{solid}}(\omega, \gamma_0)$ and $G''_{\text{fluid}}(\omega, \gamma_0)$, for Carbopol 980. By contrast, models that invoke the Oldroyd-Prager formulation [41,66,69] predict no $G''_{\text{fluid}}(\omega, \gamma_0)$ contributions below the yield stress [38] and predict abrupt changes in $G''(\omega, \gamma_0)$ when the yield stress is exceeded [57].

The nonzero values of $G''_{\text{fluid}}(\omega, \gamma_0)$ across the full range of amplitudes shown in Fig. 1 indicate that unrecoverable plastic deformation is acquired even when the stress is below the yield stress. The model allows for this by having the plastic viscosity be dependent on the total shear rate, which includes elastic deformations, $\eta_p(\dot{\gamma}) = \sigma_y/|(\dot{\gamma}_{\text{rec}} + \dot{\gamma}_{\text{unrec}})| + k|(\dot{\gamma}_{\text{rec}} + \dot{\gamma}_{\text{unrec}})|^{n-1}$. Rapid elastic

deformation (large $\dot{\gamma}_{\text{rec}}$) therefore decreases the viscosity of the unrecoverable component, η_p, which results in plastic flow at stresses lower than the steady-state yield stress.

While the model captures the behavior of the dynamic moduli, which represent an average response over a period, as observed in Fig. 1, a stricter test of the predictions can be made by examining the transient responses. We achieve this by comparing the Lissajous curves, in which the stress is plotted parametrically against the total strain, in Fig. 2. The model captures all of the features observed experimentally, including the overall shapes and the instantaneous slopes of the curves in different regions.

The transient response of the material at larger strain amplitudes can be explained as following a continuous and periodic sequence of physical processes that is made clear by examination of the instantaneous Deborah number [90]. Solidlike and fluidlike behaviors are indicated by values of the Deborah number that are greater than or smaller than unity, respectively. We define the Deborah number for oscillatory shearing as $\text{De} = t_{\text{mat}}/t_{\text{obs}} = \omega\lambda(\dot{\gamma})$, where t_{mat} and t_{obs} are material and observation times, and $\lambda(\dot{\gamma})$ is the rate-dependent relaxation time defined by Eq. (4). An oscillating relaxation time was recently observed during LAOS experiments on amorphous colloidal monolayers [81]. In our experiments and those in [81], at values of the (total) strain around zero, the shear rate is largest, the relaxation time is shortest, $\text{De} < 1$, and fluidlike behavior is observed. At the strain extrema, when the shear rate is zero, the relaxation time is infinite, $\text{De} = \infty$, and solidlike behavior is observed. Between these extremes, the model displays smooth and continuous yielding and unyielding as the relaxation time drops below or increases beyond the period of oscillation.

The response of YSFs has been studied under a variety of different protocols, and it is important to investigate the ability of any model to predict behaviors seen in a wide range of experiments. A comparison of the model's predictions and experimental data for steady-shear startup
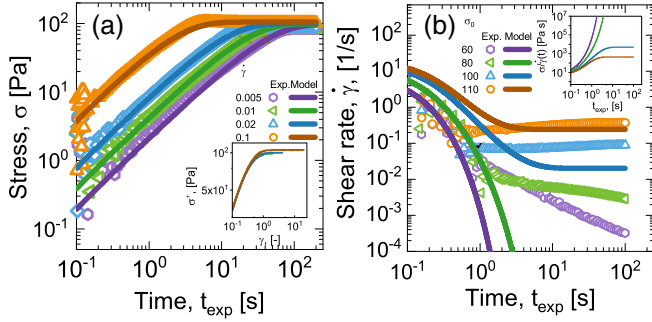
FIG. 3. (a) Comparison of experiment (symbols) and model (lines) results for steady shear startup tests at four applied shear rates. The inset shows the variation of shear stress with strain. (b) Comparison of experiment (symbols) and model (lines) results for steady creep tests at four applied stress magnitudes. The inset shows the evolution of the viscosity $[\sigma/\dot{\gamma}(t)]$. Model parameters are listed in the Supplemental Material [82].

and creep experiments on our model YSF is shown in Figs. 3(a) and 3(b).

The steady-shear startup experiments show elastic, solid-like responses at early times across the range of imposed shear rates. At long times, the sample has yielded and flows plastically, with the stress taking the steady-state value prescribed by the flow curve, $\sigma(\dot{\gamma}) = \sigma_y + k\dot{\gamma}^n$. The model predicts the same response and provides a clear physical explanation: the strain is acquired recoverably at the early times, while the unrecoverable component dominates at long times. The relevant timescale is set by the relaxation time, which is dictated by the applied shear rate. The model response for steady shear startup, where $\dot{\gamma} = $ constant and $\ddot{\gamma} = 0$, can be obtained from Eqs. (3) and (4) to show the stress is a function of strain and rate only,

$$\sigma(\dot{\gamma}, \gamma) = (\sigma_y + k|\dot{\gamma}|^n)\left[1 - \exp\left(-\frac{G\gamma}{\sigma_y + k|\dot{\gamma}|^n + \eta_s|\dot{\gamma}|}\right)\right].$$

(7)

At low shear rates, where $\sigma_y \gg k|\dot{\gamma}|^n + \eta_s|\dot{\gamma}|$, the small strain response is $\sigma = G\gamma$, showing that the stress is elastically proportional to the strain. The evolution of stress with strain is displayed in the inset in Fig. 3(a).

A yield strain γ_y, which acts as a threshold similar to the yield stress, is often measured in studies of YSFs [39,41,91]. As seen from Eq. (7), the model predicts an apparent yield strain $\gamma_y = (\sigma_y + k|\dot{\gamma}|^n + \eta_s|\dot{\gamma}|)/G$ that depends on the rate when $\sigma_y \lesssim k|\dot{\gamma}|^n + \eta_s|\dot{\gamma}|$ but is independent of the shear rate at low rates, with a value of $\gamma_y = \sigma_y/G$.

We again make use of the Deborah number, $\mathrm{De} = \lambda(\dot{\gamma})/t_{\mathrm{obs}}$, to describe the observed physics. By imposing a fixed shear rate, we are setting the relaxation time according to Eq. (4). At times shorter than this relaxation time, when $\mathrm{De} > 1$, a solidlike elastic response is elicited. Fluidlike behavior is observed when the

observation time exceeds the relaxation time. In between, smooth and continuous yielding occurs as the observation time exceeds the relaxation time.

In constant stress experiments on YSFs, the viscosity at long times has been observed to bifurcate about the yield stress with avalanches observed for stresses larger than the yield stress [26]. For imposed stresses below the yield stress, the viscosity continues to increase until the flow is halted altogether, while the viscosity remains finite for imposed stresses above the yield stress. A comparison of creep experiments and model predictions is shown in Fig. 3(b) for stresses above and below the yield stress. The creep response of the model can be determined by substituting $\dot{\sigma} = 0$ into Eq. (3):

$$\ddot{\gamma} = \left(\frac{\sigma}{\sigma_y + k|\dot{\gamma}|^n} - 1\right)\frac{G\dot{\gamma}}{\eta_s}.$$

(8)

For stresses above the yield stress, the strain rate will initially increase exponentially until reaching the steady-state value. Avalanches are therefore predicted. The model clearly captures the viscosity bifurcation shown in the inset of Fig. 3(b). In contrast to steady shear startup experiments, where the shear rate and the relaxation time are kept constant, creep experiments allow for the relaxation time to vary as the experiment progresses. This can result in a nonmonotonic evolution of the Deborah number. At imposed stresses below the yield stress, the relaxation time continuously increases with time, ensuring $\mathrm{De} > 1$ at all times. For imposed stresses larger than the yield stress, the relaxation time remains short, $\mathrm{De} < 1$, and the system flows stably at long times.

We have unified the rheological physics above and below the yield stress by constructing a continuum viscoelastic model of yield stress fluid rheology that accounts for the nonlinear rheology of a model yield stress fluid. The model is formulated so that the unrecoverable plastic viscosity is dependent on the total shear rate, which includes the rate at which strain is acquired recoverably. Plastic flow is therefore aided by the rate at which elastic deformation is acquired, and is able to occur transiently at stresses below the yield stress. At steady state, however, the elastic deformation saturates, and the total strain rate becomes equal to the unrecoverable rate. The stress therefore needs to be maintained above the yield stress for stable plastic flow to be established, which can be initiated below the yield stress.

While a single yield stress is assumed, the process of yielding is accounted for by a rate-dependent relaxation time, and can therefore be thought of as a viscoelastic process. This simple model uses parameters obtained from two steady-state tests, but accounts for a wide range of transient behaviors including the overshoot in the loss modulus observed in amplitude sweeps, the transient large amplitude oscillatory shear responses, the steady-shear start-up, and transient creep and avalanche behaviors.

The simplicity of the model also makes it a good candidate for future computational studies of YSF rheology in complex geometries.

---

*sarogers@illinois.edu

[1] D. Bonn, H. Tanaka, G. Wegdam, H. Kellay, and J. Meunier, Europhys. Lett. **45**, 52 (1999).

[2] A. Burmistrova and R. Von Klitzing, J. Mater. Chem. **20**, 3502 (2010).

[3] C. Clasen, B. P. Gearing, and G. H. McKinley, J. Rheol. **50**, 883 (2006).

[4] M. Cloitre, R. Borrega, F. Monti, and L. Leibler, Phys. Rev. Lett. **90**, 068303 (2003).

[5] M. Jalaal, G. Cottrell, N. Balmforth, and B. Stoeber, J. Rheol. **61**, 139 (2017).

[6] T. Jiang and C. F. Zukoski, Soft Matter **9**, 3117 (2013).

[7] R. C. Kramb and C. F. Zukoski, J. Rheol. **55**, 1069 (2011).

[8] M. Le Merrer, R. Lespiat, R. Höhler, and S. Cohen-Addad, Soft Matter **11**, 368 (2015).

[9] K. N. Nordstrom, E. Verneuil, P. E. Arratia, A. Basu, Z. Zhang, A. G. Yodh, J. P. Gollub, and D. J. Durian, Phys. Rev. Lett. **105**, 175701 (2010).

[10] C. S. O'Bryan, T. Bhattacharjee, S. Hart, C. P. Kabb, K. D. Schulze, I. Chilakala, B. S. Sumerlin, W. G. Sawyer, and T. E. Angelini, Sci. Adv. **3**, e1602800 (2017).

[11] J. M. Piau, J. Non-Newtonian Fluid Mech. **144**, 1 (2007).

[12] S. A. Rogers, B. M. Erwin, D. Vlassopoulos, and M. Cloitre, J. Rheol. **55**, 733 (2011).

[13] H. Senff and W. Richtering, J. Chem. Phys. **111**, 1705 (1999).

[14] J. M. Ginder, L. C. Davis, and L. D. Elie, Int. J. Mod. Phys. B **10**, 3293 (1996).

[15] X. Liu, J. Guo, Y. Cheng, G. Xu, Y. Li, and P. Cui, Rheol. Acta **49**, 837 (2010).

[16] Y. D. Liu and H. J. Choi, Soft Matter **8**, 11961 (2012).

[17] W. Mickel, S. Münster, L. M. Jawerth, D. A. Vader, D. A. Weitz, A. P. Sheppard, K. Mecke, B. Fabry, and G. E. Schröder-Turk, Biophys. J. **95**, 6072 (2008).

[18] A. R. Patel, B. Mankoč, M. D. Bin Sintang, A. Lesaffer, and K. Dewettinck, RSC Adv. **5**, 9703 (2015).

[19] P. J. Rankin, A. T. Horvath, and D. J. Klingenberg, Rheol. Acta **38**, 471 (1999).

[20] H. J. Walls, S. B. Caines, A. M. Sanchez, and S. A. Khan, J. Rheol. **47**, 847 (2003).

[21] H. G. Yang, C. Z. Li, H. C. Gu, and T. N. Fang, J. Colloid Interface Sci. **236**, 96 (2001).

[22] C. F. Zukoski and D. J. Klingenberg, Langmuir **6**, 15 (1990).

[23] T. Divoux, D. Tamarii, C. Barentin, and S. Manneville, Phys. Rev. Lett. **104**, 208301 (2010).

[24] T. Gibaud, C. Barentin, and S. Manneville, Phys. Rev. Lett. **101**, 258302 (2008).

[25] A. Kurokawa, V. Vidal, K. Kurita, T. Divoux, and S. Manneville, Soft Matter **11**, 9026 (2015).

[26] P. Coussot, Q. D. Nguyen, H. T. Huynh, and D. Bonn, Phys. Rev. Lett. **88**, 175501 (2002).

[27] T. Bauer, J. Oberdisse, and L. Ramos, Phys. Rev. Lett. **97**, 258303 (2006).

[28] T. Sentjabrskaja, P. Chaudhuri, M. Hermes, W. C. Poon, J. Horbach, S. U. Egelhaaf, and M. Laurati, Sci. Rep. **5**, 11884 (2015).

[29] M. Siebenbürger, M. Ballauff, and T. Voigtmann, Phys. Rev. Lett. **108**, 255701 (2012).

[30] J. Sprakel, S. B. Lindström, T. E. Kodger, and D. A. Weitz, Phys. Rev. Lett. **106**, 248303 (2011).

[31] D. Bonn and M. M. Denn, Science **324**, 1401 (2009).

[32] K. Hyun, S. H Kim, K. H Ahn, and S. J Lee, J. Non-Newtonian Fluid Mech. **107**, 51 (2002).

[33] A. R. Payne, J. Appl. Polym. Sci. **6**, 57 (1962).

[34] H. M. Wyss, K. Miyazaki, J. Mattsson, Z. Hu, D. R. Reichman, and D. A. Weitz, Phys. Rev. Lett. **98**, 238303 (2007).

[35] T. G. Mason and D. A. Weitz, Phys. Rev. Lett. **75**, 2770 (1995).

[36] T. G. Mason, M. D. Lacasse, G. S. Grest, D. Levine, J. Bibette, and D. A. Weitz, Phys. Rev. E **56**, 3150 (1997).

[37] T. G. Mason, J. Bibette, and D. A. Weitz, Phys. Rev. Lett. **75**, 2051 (1995).

[38] G. J. Donley, P. K. Singh, A. Shetty, and S. A. Rogers, Proc. Natl. Acad. Sci. U.S.A. **117**, 21945 (2020).

[39] M. Dinkgreve, J. Paredes, M. M. Denn, and D. Bonn, J. Non-Newtonian Fluid Mech. **238**, 233 (2016).

[40] G. J. Donley, J. R. de Bruyn, G. H. McKinley, and S. A. Rogers, J. Non-Newtonian Fluid Mech. **264**, 117 (2019).

[41] M. Dinkgreve, M. M. Denn, and D. Bonn, Rheol. Acta **56**, 189 (2017).

[42] P. Hébraud, F. Lequeux, J. P. Munch, and D. J. Pine, Phys. Rev. Lett. **78**, 4657 (1997).

[43] E. D. Knowlton, D. J. Pine, and L. Cipelletti, Soft Matter **10**, 6931 (2014).

[44] L. Bécu, S. Manneville, and A. Colin, Phys. Rev. Lett. **96**, 138302 (2006).

[45] T. Gibaud, D. Frelat, and S. Manneville, Soft Matter **6**, 3482 (2010).

[46] T. Gibaud, C. Barentin, and S. Manneville, Phys. Rev. Lett. **101**, 258302 (2008).

[47] T. Divoux, D. Tamarii, C. Barentin, S. Teitel, and S. Manneville, Soft Matter **8**, 4151 (2012).

[48] M. C. Rogers, K. Chen, L. Andrzejewski, S. Narayanan, S. Ramakrishnan, R. L. Leheny, and J. L. Harden, Phys. Rev. E **90**, 062310 (2014).

[49] M. C. Rogers, K. Chen, M. J. Pagenkopp, T. G. Mason, S. Narayanan, J. L. Harden, and R. L. Leheny, Phys. Rev. Mater. **2**, 095601 (2018).

[50] B. Ferdowsi, C. P. Ortiz, and D. J. Jerolmack, Proc. Natl. Acad. Sci. U.S.A. **115**, 4827 (2018).

[51] S. Karmakar, A. Lemaître, E. Lerner, and I. Procaccia, Phys. Rev. Lett. **104**, 215502 (2010).

[52] J. Lin, E. Lerner, A. Rosso, and M. Wyart, Proc. Natl. Acad. Sci. U.S.A. **111**, 14382 (2014).

[53] J. D. Paulsen, N. C. Keim, and S. R. Nagel, Phys. Rev. Lett. **113**, 068301 (2014).

[54] G. Petekidis, A. Moussaïd, and P. N. Pusey, Phys. Rev. E **66**, 051402 (2002).

[55] R. Zondervan, T. Xia, H. Van Der Meer, C. Storm, F. Kulzer, W. Van Saarloos, and M. Orrit, Proc. Natl. Acad. Sci. U.S.A. **105**, 4993 (2008).

[56] N. C. Keim and P. E. Arratia, Phys. Rev. Lett. **112**, 028302 (2014).

[57] P. Saramito, J. Non-Newtonian Fluid Mech. **145**, 1 (2007).

[58] E. Bingham, *Fluidity and Plasticity* (McGraw-Hill, New-York, USA, 1922).

[59] W. H. Herschel and R. Bulkley, Kolloid-Zeitschrift **39**, 291 (1926).

[60] N. Casson, in *The Rheology of Disperse Systems*, edited by C. C. Mill (Pergamon Press, London, 1959), Chap. 5.

[61] M. Caggioni, V. Trappe, and P. T. Spicer, J. Rheol. **64**, 413 (2020).

[62] K. N. Nordstrom, E. Verneuil, P. Arratia, A. Basu, Z. Zhang, A. G. Yodh, J. P. Gollub, and D. J. Durian, Phys. Rev. Lett. **105**, 175701 (2010).

[63] J. Paredes, M. A. Michels, and D. Bonn, Phys. Rev. Lett. **111**, 015701 (2013).

[64] C. Pellet and M. Cloitre, Soft Matter **12**, 3710 (2016).

[65] A. Basu, Y. Xu, T. Still, P. Arratia, Z. Zhang, K. Nordstrom, J. M. Rieser, J. Gollub, D. Durian, and A. Yodh, Soft Matter **10**, 3027 (2014).

[66] J. G. Oldroyd, Proc. Cambridge Philos. Soc. **43**, 100 (1947).

[67] P. Saramito, J. Non-Newtonian Fluid Mech. **158**, 154 (2009).

[68] K. Hohenemser and W. Prager, Angew. Math. Mech. **12**, 216 (1932).

[69] W. Prager, *Introduction to Mechanics of Continua* (Ginn & Co., Boston, 1961).

[70] M. Bercovier, M. Engelman, and M. Fortin, J. Comput. Phys. **36**, 313 (1980).

[71] D. K. Gartling and N. Phan-Thien, J. Non-Newtonian Fluid Mech. **14**, 347 (1984).

[72] G. G. Lipscomb and M. M. Denn, J. Non-Newtonian Fluid Mech. **14**, 337 (1984).

[73] T. C. Papanastasiou, J. Rheol. **31**, 385 (1987).

[74] K. Weissenberg, Nature (London) **159**, 310 (1947).

[75] M. Reiner, *Encyclopedia of Physics VI* (Springer-Verlag, Berlin, 1958).

[76] M. H. Wagner and H. M. Laun, Rheol. Acta **17**, 138 (1978).

[77] H. M. Laun, J. Rheol. **30**, 459 (1986).

[78] J. C. W. Lee, K. M. Weigandt, E. G. Kelley, and S. A. Rogers, Phys. Rev. Lett. **122**, 248003 (2019).

[79] N. W. Tschoegl, *The Phenomenological Theory of Linear Viscoelastic Behavior* (Springer, Berlin Heidelberg, 1989).

[80] P. Sollich, Phys. Rev. E **58**, 738 (1998).

[81] K. Lawrence Galloway, X. Ma, N. C. Keim, D. J. Jerolmack, A. G. Yodh, and P. E. Arratia, Proc. Natl. Acad. Sci. U.S.A. **117**, 11887 (2020).

[82] See Supplemental Material at http://link.aps.org/supplemental/10.1103/PhysRevLett.126.218002 for tensorial model formulation, material preparation details, and experimental data and model comparisons for additional YSFs, which includes Refs. [32,40,83,84].

[83] P. R. de Souza Mendes, Soft Matter **7**, 2471 (2011).

[84] S. A. Rogers, J. D. Park, and C.-W. J. Lee, Rheol. Acta **58**, 539 (2019).

[85] H. De Cagny, M. Fazilati, M. Habibi, M. M. Denn, and D. Bonn, J. Rheol. **63**, 285 (2019).

[86] M. B. Gordon, C. J. Kloxin, and N. J. Wagner, J. Rheol. **61**, 23 (2017).

[87] P. Moller, A. Fall, V. Chikkadi, D. Derks, and D. Bonn, Philos. Trans. R. Soc. A Math. Phys. Eng. Sci. **367**, 5139 (2009).

[88] E. E. Ong, S. O'Byrne, and J. L. Liow, Rheol. Acta **58**, 383 (2019).

[89] J. Carnali, J. Appl. Polym. Sci. **43**, 929 (1991).

[90] M. Reiner, Phys. Today **17**, No. 1, 62 (1964).

[91] R. R. Fernandes, D. E. V. Andrade, A. T. Franco, and C. O. R. Negrão, Rheol. Acta **56**, 743 (2017).